



A 3D printing tool-path generation strategy based on the partition of principal stress field for fused filament fabrication

Hang Zhang¹ · Yuan Yao^{2,3} · Yingxin Ma¹ · Maximilian Lackner⁴ · Yunliang Jiang⁵

Received: 8 March 2022 / Accepted: 12 August 2022 / Published online: 25 August 2022

© The Author(s), under exclusive licence to Springer-Verlag London Ltd., part of Springer Nature 2022

Abstract

In order to enhance the strength of 3D-printed parts made of polymer materials and reduce the anisotropy caused by the fused filament fabrication process, this paper proposes an inter-layer interleaved composite path planning method based on the directional partition of the principal stress field. This method not only ensures intra-layer reinforcement under specific working conditions but also increases the strength of the printed part by enhancing the adhesion of adjacent layers through staggered filling between layers. The mechanical performance is improved by 10 to 30% compared to other conventional filling patterns such as the zigzag filling algorithm. Inter-layer interleaved composite enhancement path planning method is suitable for path planning of structures with complex shapes and is easily integrated into existing general computer-aided engineering processes.

Keywords Principal stress field · Anisotropy strength · Clustering · FFF

1 Introduction

Additive manufacturing (AM) technology also referred to as 3D printing is an assisted manufacturing method for creating model data of different components and complex shapes. These model data are mainly modeled by computer-aided design (CAD) and then converted into triangle mesh for printing [1]. With the increasing maturity of AM technology, 3D printing technologies such as selective laser sintering (SLS), stereo lithography appearance (SLA), fused filament fabrication (FFF), and laminated object manufacturing (LOM) [2] have emerged and these techniques have important applications in technical industrial design, architecture, aerospace, and medical fields [3, 4]. The FFF process has become the most widely used process in AM technology due to its inexpensive equipment, easy handling, and low cost of production and printing materials. This process is mainly printed by heating the print nozzle and feeding the polymer filament through the roller into the nozzle in cumulative layers [5, 6]. The strength and surface quality of parts fabricated by the FFF process is affected by various processing parameters and path planning factors, such as layer thickness, nozzle diameter, filling spacing, printing temperature, printing speed, different polymer materials, and material extrusion rate, filling strategy, etc. The presence of these influencing factors makes it difficult to use

✉ Yuan Yao
yaoyuan@shu.edu.cn

Hang Zhang
1054506202@qq.com

Yingxin Ma
3051998634@qq.com

Maximilian Lackner
lacknerm@technikum-wien.at

Yunliang Jiang
jyl@zjhu.edu.cn

¹ School of Mechatronic Engineering and Automation, Shanghai University, 99 Road Shanda, Shanghai 200444, China

² Engineering Training Center, Shanghai University, 99 Road Shanda, Shanghai 200444, China

³ Shanghai Key Laboratory of Intelligent Manufacturing and Robotics, Shanghai University, 99 Road Shanda, Shanghai 200444, China

⁴ University of Applied Sciences Technikum Wien, Höchstädtplatz 6, Vienna 1200, Austria

⁵ Huzhou University, 759 2nd Ring East Road, Huzhou 313000, China

the FFF process directly in the manufacture of structural and load-bearing parts. The main constraints are the strength and surface quality of the printed part [7, 8]. In order to solve these problems, some researchers have tried to greatly improve the quality of the printed parts by the FFF process by optimizing these parameters that affect the printing quality and enhancing the connection between the printed filaments and the adhesion between the layers, which can considerably reduce the anisotropy of the printed parts brought by the FFF process [9–12]. Based on the different types of implementation, these methods can be broadly divided into two parts, process parameters and path planning.

The process parameters are mainly aimed at enhancing the mechanical properties of the part by strengthening the fragile connection between adjacent filaments and reducing the porosity. The layer thickness and nozzle diameter mainly affect the surface quality of the molded part. Lower layer thickness means better denseness of the molded part, relatively smaller pores, and higher surface quality [13]. The printing temperature, material extrusion rate, and printing speed [14–16] affect the printing quality mainly by the flow rate of the filament under melting. In addition, different polymer materials for printing can lead to large differences in mechanical properties [17]. Another way of enhancing the strength of the part is to change the printing path by different filling strategies such as direction and parallel [18], and spiral curves [19], and Hibert curves [20], and hybrid curves [21], and maze-like [22], contour and parallel curves [23], and connected Fermat spiral [24]. However, when the printed part is subjected to external loads, the anisotropy caused by the printing path will lead to the weakening of the load-bearing capacity of the component and the occurrence of damage. Several studies have found that when filling with different directional paths, it can not only compensate for the porosity resulting from a single filling method but also effectively reduce the anisotropy of the workpiece and enhance its strength. When especially manufactured with the direction of the force, the enhancement effect can reach its peak [25]. So making the printing path along the load-bearing direction of the structure has become a key research point for path planning. But subsequently, it will also pose many problems. A single force field driving not only increases the anisotropy within and between layers but also reduces the stability of the process. Inconsistent path planning creates more porosity in the printed part, which in turn reduces the surface quality and mechanical strength of the fabricated part.

In this paper, we propose a new inter-layer interleaved composite enhancement path planning method (IICP) to realize the generation of enhanced printing paths for arbitrary working conditions based on the partition of the principal stress direction. IICP can not only enhance the mechanical properties of printings but also reduce the anisotropy of the part by inter-layer staggered printing, which improves the practical performance of the FFF process.

2 Related works

The current FFF path optimization method can be divided into two major directions. The first is the use of topology optimization to present the main load-bearing areas of the structure by dense filling in key areas. It not only can enhance the mechanical properties by improving the stiffness of the structure but also effectively reduce the weight of the structure [26]. This designing method generally uses commercial software for auxiliary analysis. Firstly, it carries out modeling through CAD, and then performs the advanced simulation function of the software. By simulating realistic operating conditions, adding loads, constraints, and boundary conditions, and sometimes taking into account material anisotropy. An optimized CAD model is generated by setting the objective function. Then, the model is sliced and converted into a 2D planar model. The inward and outward contours are filled with offsets on the planar surface. Papapetrou et al. [27] proposed two new topology optimization methods to achieve variable stiffness design and optimize the material distribution. Different filling strategies are also given for the two different optimization methods, linear filling and contour biasing.

The other one is based on the filling of the principal stress field direction of the structure. According to the actual working conditions, the second-order Cauchy stress tensor of the node is obtained by finite element analysis. Then, the eigenvalue and eigenvector are calculated. The eigenvalue is the magnitude of the principal stress at the node, and the eigenvector is the direction of the principal stress. The load-bearing capacity of the structure is enhanced by aligning the printed filaments in the direction of the principal stress [28]. The current study found that this filling method generally uses a two-dimensional structure, where N seed points are first selected randomly in the plane, and these seed points are used as the points to be connected. The magnitudes and directions of principal stress of the seed points are calculated by using interpolation [29]. Sales et al. [30] used the optimized principal stress line (PSL) as the printing path based on the finite element analysis, combining CAD and CAM for the first time, not only considering the enhancement effect of the structure but also conforming to the actual machining process. Li et al. [31] first used grayscale images to represent irregular vector fields that can be processed into regular print paths in sub-regions utilizing image processing. Jin et al. [32] introduced a new continuous path filling scheme that fully decreases the printer start-stop process and reduces the process complexity. This article uses a “go and back” path strategy to improve the shortcomings of the traditional zigzag filling curve discontinuity, achieving continuous Z-printing and effectively reducing printing time. This approach gives a new continuous path planning method for force field layout but does not have a significant strength enhancement. These studies based on

primary stress field printing do not take into account the practical impact of inter-layer path enhancement on the process.

If the layers are printed along a mono stress direction, the component may fracture weakly on the other side in practice, which in turn can significantly reduce the strength of the component. The key to inter-layer reinforcement is how to improve the matrix bonding between the layers, which has a significant effect on enhancing the lateral force of the printed parts. Since there is a certain gap between the printed and unprinted layers, the matrix of the unprinted layer can be deposited inside the printed layer through the gap by adjusting the printing direction of the adjacent layers. So, when the printed matrix is solidified, the connecting strength of the adjacent layers will be enhanced [33]. McLouth et al. [34] investigated the effect of different raster angles on the performance of printed parts. The experimental results show that when the filling direction alternates at $-45^\circ / +45^\circ$, the breaking strength is the strongest and the fracture crack is the shortest. This article prevents crack expansion by adjusting the construction direction of the model so that the crack expansion direction is perpendicular to the printing direction when a fracture occurs in the printed part. However, this method of enhancing fracture strength is only applicable to particular printed models for specific working conditions.

The above path planning methods either only consider the enhancement effect in the plane and do not take into account the inter-layer enhancement, or they do not consider the anisotropy of the filament printing due to the FFF process, resulting in limited improvement of the mechanical properties of the printed parts. The IICP method proposed in this paper uses the stress field generated under specific working conditions to perform global path planning.

3 Method

Since the path arrangement based on the stress field generated by the specific working conditions can easily increase the anisotropy of the printed part, therefore, the main idea of the IICP method is to divide the sliced layers into planar reinforced layers and processing transitional layers. The stress field driving method is used within the enhancement layer to generate planar paths. Perpendicular paths are used in the transitional layer for inter-layer enhancement. The IICP method can be applied to general engineering conditions and complex models. However, it should be noted that the stress field varies drastically from element to element, so printing along the direction of the stress field is not possible in practical applications, and a printing path completely aligned with the stress field will not only increase the porosity of the printed part and reduce the surface quality but also make the FFF process becomes complicated. The IICP method estimates the approximate direction of the local stress field, divides the fill plane into different regions, and adjusts the area size by different thresholds. This

approach can reduce the difficulty of process implementation while ensuring mechanical properties.

As shown in Fig. 1, IICP is divided into three steps: (1) pre-processing, (2) planar path planning, and (3) global path planning.

3.1 Pre-processing

Pre-processing is used to calculate the real force state in the physical world through CAD modeling. Finite element analysis (FEA) and other methods are deployed to generate the approximate internal force of the object in the volumetric space. It mainly consists of two parts: (1) volumetric model conversion and (2) stress field generated by the FEA process. In the first step, the three-dimensional model is volumized and added with the corresponding constraints and loads based on the requirements of the special case. And then the stress field of the finite element model is generated to be used for subsequent analysis.

3.2 Planar path planning

The planar path planning method is mainly to map the stress field of a 3D finite element to the characteristic points of a 2D plane through slicing. Then, the principal stress field is lined up and used for filling in the 2D plane. It mainly consists of the following steps: slicing, partitioning, and filling.

Firstly, the 3D data model is converted to the 2D plane by slicing, and then the stress characteristic points for planar path planning are selected on the 2D plane by the triangulation method. Since the stress fields of the characteristic points obtained from the finite element calculations are scattered on the planar region and the stress fields vary drastically between adjacent points. If the printing is completely along the principal stress direction of the characteristic points, it will cause the unevenness in the printing path and there is no way to control the density of the printing, resulting in high porosity and poor printing quality. So we use a planar partitioning approach to cluster these feature points with similar principal stress directions into a large region, and then use this large region as a separate filling region. This not only separates stress-concentrated areas from less-stressed areas but also controls the filling rate of the printing. Finally, we can divide the plane into different regions according to the difference in the direction of the plane stress field, and each region has a printing reference direction for zigzag filling. This ensures that each area is filled in such a way that the load is carried in the direction of the principal stress, thus maximizing the strength of the printed part.

3.3 Global path planning

Based on the planar path planning of Sect. 3.2, in order to improve the practical performance of the process and

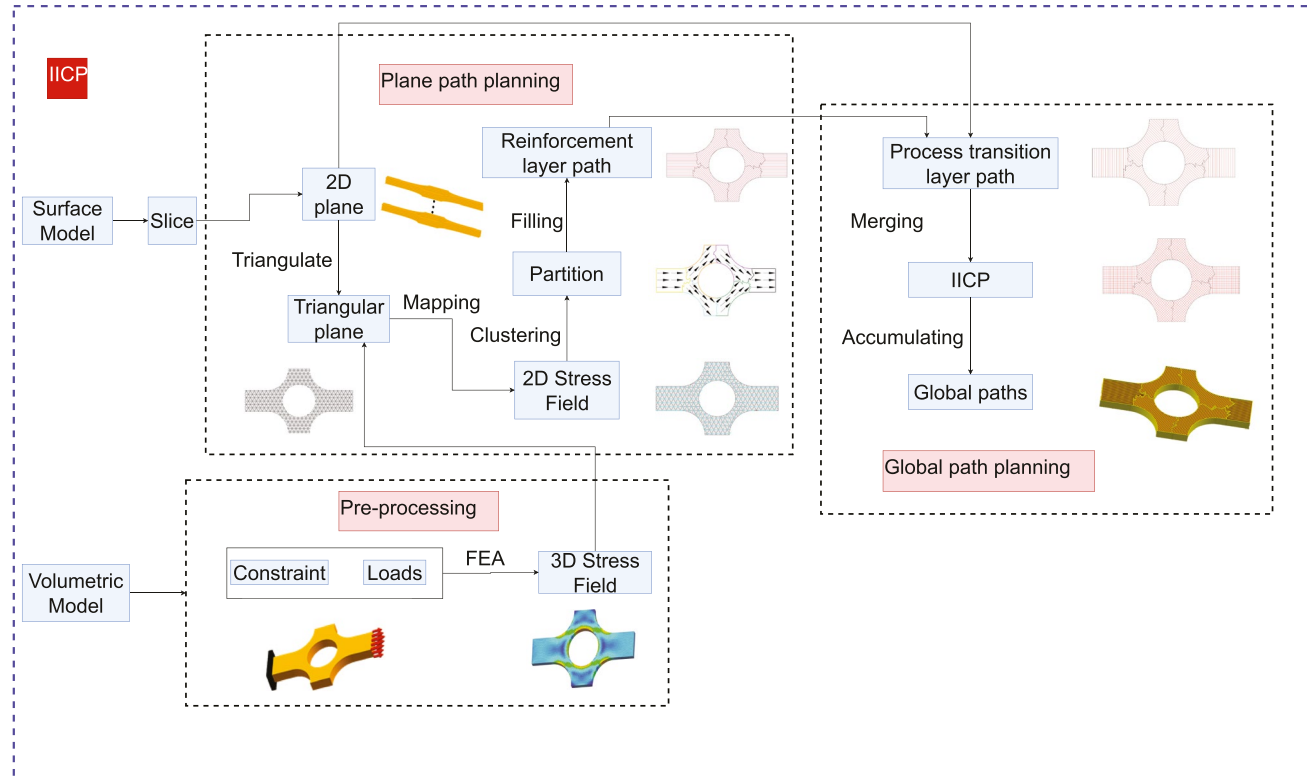


Fig. 1 Framework overview for applying IICP method in tool-path planning

reduce the anisotropy of the FFF process, the layers are processed with vertically staggered filling with the reinforced layers. This strategy is mainly to increase the contacting area of adjacent layers and reduce the porosity from the single-layer directional filling method. The vertically staggered filling of adjacent layers allows the matrix of the unprinted layer to be impregnated into the printed layer through the interlaminar gap, which effectively strengthens the interlaminar bond and increases the interlaminar strength as shown in Fig. 2.

4 Force field–driven planar path planning

From the designing principle proposed by Fang et al. [35], it can be concluded that the strength of the printed part of the FFF process is highly dependent on the direction of the printing path. For samples printed perpendicular to the tension direction, its yield strength is 25% lower than for those printed parallel to the tension direction. As a result, the mechanical strength of the printed part can be significantly enhanced when printing in the direction of the force. Therefore, this polymer-reinforced printing path direction is used as a guide for the layout of Sect. 3.2.

4.1 Principal stress field analysis

$$\sigma_{ij} = \begin{bmatrix} \sigma_{11} & \sigma_{12} & \sigma_{13} \\ \sigma_{21} & \sigma_{22} & \sigma_{23} \\ \sigma_{31} & \sigma_{32} & \sigma_{33} \end{bmatrix} \quad (1)$$

$$\begin{aligned} (\sigma_{11} - \sigma_v)v_1 + \sigma_{21}v_2 + \sigma_{31}v_3 &= 0 \\ \sigma_{12}v_1 + (\sigma_{22} - \sigma_v)v_2 + \sigma_{32}v_3 &= 0 \\ \sigma_{13}v_1 + \sigma_{23}v_2 + (\sigma_{33} - \sigma_v)v_3 &= 0 \end{aligned} \quad (2)$$

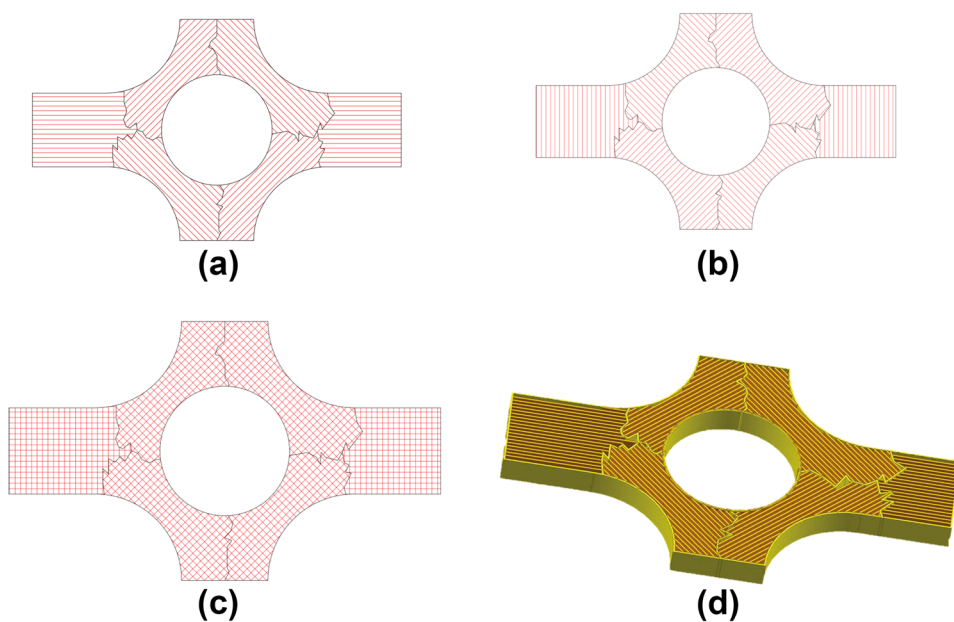
Here, σ_{ij} denotes the stress tensor of a point, and three invariants of the stress tensor can be obtained through the expression of this matrix.

The system of linear equations for solving the principle direction \vec{v} is obtained from the formula $\vec{v} \cdot \vec{\sigma} = \sigma_v \vec{v}$ as shown in Eq. 2

The three invariants of the stress tensor are obtained from Eq. 1, and their values are independent of the selection of coordinates.

$$\begin{aligned} I_1 &= \sigma_{11} + \sigma_{22} + \sigma_{33} \\ I_2 &= \sigma_{11}\sigma_{22} + \sigma_{22}\sigma_{33} + \sigma_{33}\sigma_{11} - \sigma_{12}^2 - \sigma_{23}^2 - \sigma_{31}^2 \\ I_3 &= \begin{vmatrix} \sigma_{11} & \sigma_{12} & \sigma_{13} \\ \sigma_{21} & \sigma_{22} & \sigma_{23} \\ \sigma_{31} & \sigma_{32} & \sigma_{33} \end{vmatrix} \end{aligned} \quad (3)$$

Fig. 2 Schematic diagram of global path planning. **a** Planar enhancement layer filling paths. **b** Processing transitional layer filling paths. **c** IICP. **d** Global filling paths



So according to Eq. 3,

$$\begin{aligned}\sigma_{(1)} &= \sigma_0 + \sqrt{2}\tau_0 \cos \theta \\ \sigma_{(2)} &= \sigma_0 + \sqrt{2}\tau_0 \cos(\theta + \frac{2}{3}\pi) \\ \sigma_{(3)} &= \sigma_0 + \sqrt{2}\tau_0 \cos(\theta - \frac{2}{3}\pi)\end{aligned}\quad (4)$$

where,

$\sigma_{(i)}$ ($i = 1, 2, 3$) denotes the magnitude of the principal stress in the three directions of a point. The directions of the three principal stresses $v_{(i)}$ can be calculated by Eq. 2.

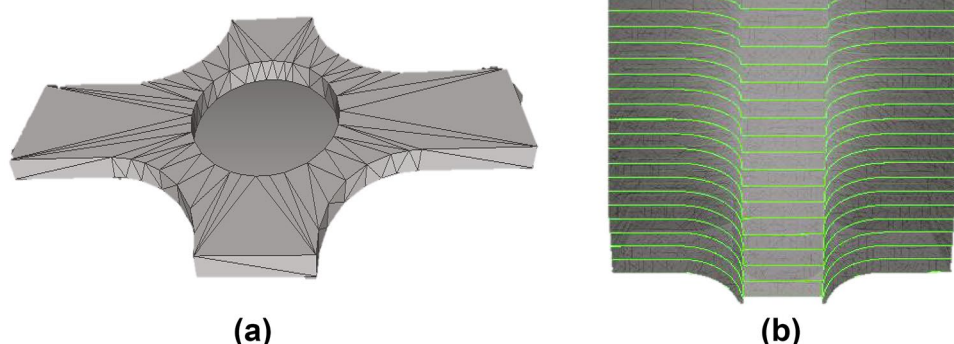
4.2 Slicing and partitioning

The FFF process uses layer-by-layer accumulation to print 3D solids. So if you want to achieve enhanced printing of structures through path planning, you need to convert the 3D model to a 2D plane by slicing. The 3D model under actual working conditions is first created by CAD software and converted into a triangle mesh model, and saved in STL

format. The contour of the tangent plane is obtained by intersecting the plane with the triangular meshes in STL. Finally, the coordinates of the vertex are together connected according to the counterclockwise outer and clockwise inner contour to form a closed outer contour [36] as shown in Fig. 3. The purpose of partition is mainly to realize the division of the plane and form a combined principal stress field by merging the scattered stress fields. This ensures that the filling inside the partition is along the principal stress direction, thus enabling enhanced path filling of the entire tangent plane. The algorithm for partition consists of three main steps.

- Partition
 - (a) Generation of the stress field for planar triangular elements.
 - (b) Clustering of triangular elements.
 - (c) Generation of the zoning contours.

Fig. 3 Process of slicing. **a** STL model generated from CAD model. **b** Cutting plane according to specific layer height



4.2.1 Generation of the stress field for planar triangular elements

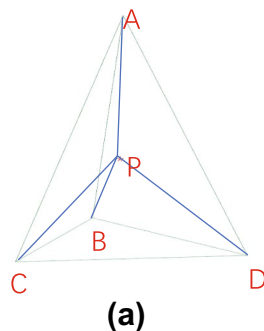
The stress field of the planar triangular element is obtained by calculating the combined stress field of the nodes. Firstly, you need to correspond the position of the triangular element nodes to the corresponding 3D finite element. Then, the stress field of the triangular node is calculated by linear interpolation of the stress tensor of the finite element node. As shown in Fig. 4(a), the point P is a node of a triangular element located inside the tetrahedron, and A, B, C, and D are nodes of the tetrahedron element. Then, the volume of the four tetrahedra formed by the point P and A, B, C, and D is calculated by Eq. 5 as V_{PABC} , V_{PABD} , V_{PBCD} , V_{PACD} . The volumetric sum is used by Eq. 6 to determine whether the point P is in the tetrahedron ABCD. If Eq. 6 is satisfied, it means that the point is located in the interior or at the edge of this tetrahedron. Then, the interpolating coefficients are computed according to the following formula $\lambda_1 = V_{PABC}/V_{ABCD}$, $\lambda_2 = V_{PABD}/V_{ABCD}$, $\lambda_3 = V_{PBCD}/V_{ABCD}$, $\lambda_4 = V_{PACD}/V_{ABCD}$. The above equation uses the volume coordinate system. So, the interpolating coefficient is the shape function of the tetrahedron element and the stress at any point inside the tetrahedron can be obtained according to the shape function. The stress tensor at this point P is $\sigma_P = \lambda_1 \times \sigma_D + \lambda_2 \times \sigma_C + \lambda_3 \times \sigma_A + \lambda_4 \times \sigma_B$.

$$V_{ABCD} = \begin{vmatrix} x_A & y_A & z_A & 1 \\ x_B & y_B & z_B & 1 \\ x_C & y_C & z_C & 1 \\ x_D & y_D & z_D & 1 \end{vmatrix} \quad (5)$$

$$V_{PABC} + V_{PABD} + V_{PBCD} + V_{PACD} = V_{ABCD} \quad (6)$$

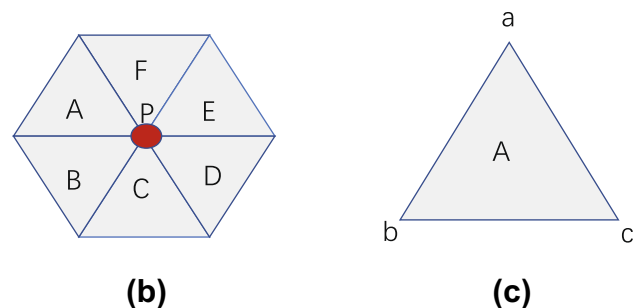
The second-order stress tensor at each node is obtained by traversing the entire triangular nodes on the tangent plane. The next step is to calculate the joint stress tensor for each triangular element node. Figure 4(b) shows that the point P is surrounded by six triangles A, B, C, D, E, and F. Before calculating the joint stress tensor of the triangles, it is necessary to calculate the stress tensor of each triangular node.

Fig. 4 Schematic diagram of stress field calculating. **a** The point is inside the tetrahedron. **b** The point is surrounded by those tetrahedrons. **c** Stress of a triangular mesh



The nodal stress tensor averaged over the above is equal to $\sigma_{A(P)} = \sigma_{B(P)} = \sigma_{C(P)} = \sigma_{D(P)} = \sigma_{E(P)} = \sigma_{F(P)} = \sigma_P/n$. So, $\sigma_A = \sigma_{A(a)} + \sigma_{A(b)} + \sigma_{A(c)}$. Figure 4(c) shows that points a, b, and c are the nodes of a triangular mesh. $\sigma_{A(a)}$, $\sigma_{A(b)}$, $\sigma_{A(c)}$ denote the stress tensor of the triangular nodes, and σ_A denotes the joint stress tensor of the triangular element. The direction and magnitude of the principal stresses in the triangular mesh can be obtained from the combined stress tensor of the triangular mesh according to the theoretical analysis in Sect. 4.1. The stress field of the whole plane can be obtained by traversing the whole triangular element.

After the initial stress field is obtained, the principal stress field varies more drastically at the border. This can lead to too small subdivided contours in the clustering process. This results in a larger number of partitions, smaller zoning contour areas, longer printing empty traveling times, and poorer printing quality. Moreover, the IICP method uses an approximate path planning printing along the principal stress field, so the generated stress field has some errors, and we need to perform smoothing on the initial stress field. First, the direction and magnitude of the principal stress for each triangular meshes correspond to its geometric center, and then the approximate nearest neighbor (ANN) method is used to search for some triangles nearest to it. Finally, the distance from the geometric center of the nearest neighboring triangle to the target point is used as the dimensional scale, and the weighted calculation finally yields the optimized direction of the stress field. As shown in Fig. 5, the green point indicates the target point P. The red points indicate the geometric centroid of the triangle in the nearest domain of point P. l indicates the distance from point P to point A. R denotes the radius of the circle with the point P as the center point of circle and its value is $r = \lambda \times \max\{PA_i\}$. The value of λ is mainly used to adjust the size of this circle and the weight of the principal stress direction of the point A. The value of $1.2 \sim 1.5$ is verified by the experiment. The stress field after optimization is obtained from Eq. 7, where n denotes the number of points in the point set A and α_i characterizes the proximity of the points in the point set A to the target point P. τ_p is the direction of the final computed stress field. The stress field after smoothing is shown in Fig. 6(b).



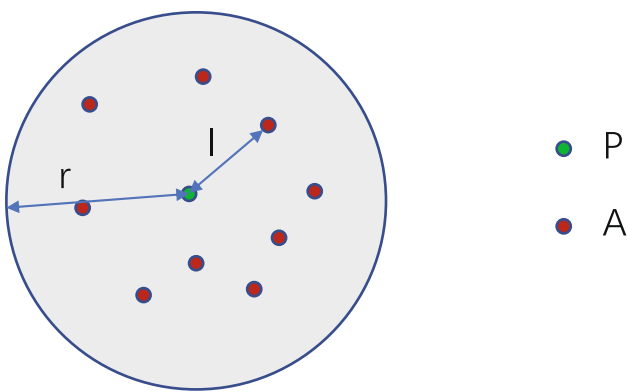


Fig. 5 Schematic diagram of distance weighting

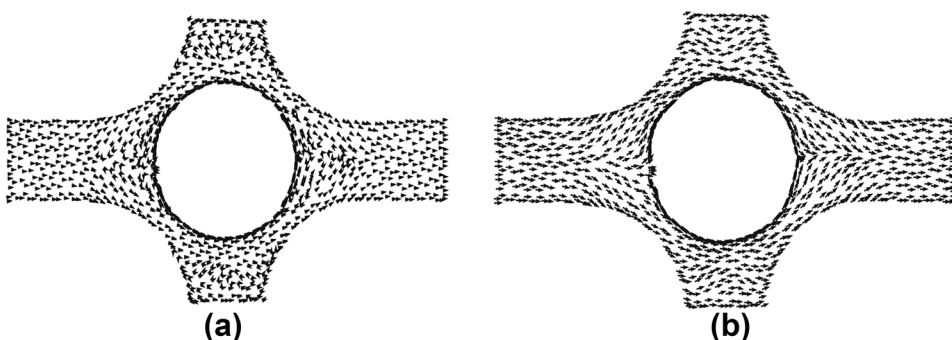
$$\begin{aligned} s &= \sum_{i=1}^n r - PA_i + r \\ \alpha_i &= (r - PA_i)/s \\ \tau_p &= \sum_{i=1}^n \alpha_i \tau_i + (1 - \sum_{i=1}^n \alpha_i) \tau_p \end{aligned} \quad (7)$$

4.2.2 Clustering of triangular elements

After the optimization of the stress field, we can cluster the triangular mesh according to the direction and magnitude of the planar stress field. The principle of clustering has two aspects. The first must ensure that the triangular meshes clustered together are adjacent to each other. The second must satisfy Eq. 8, that is, the direction of the principal stress field of the triangles clustered together with the reference direction of the region within a certain range of angular difference. The $\tau(e)$ in Eq. 8 indicates the reference direction when clustering regions. The angular difference between the direction of principal stress and the reference direction for each triangular meshes must be less than α .

$$|\tau(e) \cdot \tau(e_i)| > \alpha \quad (8)$$

Fig. 6 Schematic diagram of stress smoothing. **a** Stress field before smoothing. **b** Stress field after smoothing



Triangular meshes clustered use the conventional k-means method, but the k-means clustering method has some defects such as its clustering effect is greatly related to the initial selection of the cluster centroid. To avoid this drawback, the first step needs to find the reference direction of the initial partition before the clustering process starts. By observing the distribution of the stress field, we can roughly divide the plane into N regions. Then, the initial iterative reference direction x_i is obtained according to the equation $x_i = i \times 2\pi/N (i = 1, N)$, and v_j denotes the principal stress direction of the triangular mesh. In the second step, the triangles are placed into the region closest to their initial reference direction, and it is not necessary to satisfy the principle of clustering because this step is only looking for the initial direction of each clustering region. Then, the triangles can be placed into different partitions on the plane according to the second rule by traversing the entire triangular meshes. In the third step, the second step is repeated until the angle of the reference direction does not change. At this point, x_i is used as the reference direction of the regional clustering that is $\tau(e)$. The fourth step divides the triangular meshes on the plane into different regions according to the clustering principle as shown in Fig. 7.

$$\max_{1 \leq i \leq N} |y_i - x_i| < \varepsilon \quad (9)$$

- The process of clustering

- (a) Firstly, inputting the initial partitioned iterative reference direction x_i and the direction v_j of principal stress field of the triangular meshes.
- (b) In accordance with the principle of similarity of direction of principal stress field, it will put the triangular meshes into the corresponding partitions.
- (c) Recalculating the reference direction y_i for each partition.
- (d) If Eq. 9 is satisfied, then x_i is used as the final clustering reference direction. If not, it needs to skip this step b) and continue to update the x_i until Eq. 9 is established.

- (e) The triangular meshes on the plane are divided into different regions according to the generated reference directions and two clustering principles.

Algorithm 1 Generate the contour of regions

```

Require: triangles[1, n]
Ensure: RegionContours[1, N]
1: RegionSegments           ←
   ConvertTrianglesToSegs(triangles)
2: Contours ← []
3: for each segs ∈ RegionSegments do
4:   PolygonOne ← map < int, int >
5:   PolygonTwo ← map < int, int >
6:   for eachseg ∈ segs do
7:     PolygonOne.push_back(pair
      int, int > (seg.A, seg.B))           <
8:     PolygonTwo.push_back(pair
      int, int > (seg.B, seg.A))           <
9:   end for
10:  Contour ← []
11:  Contour.push_back(seg[0].A)
12:  Contour.push_back(seg[0].B)
13:  temp ← seg[0].B
14:  while Contour.size() = Segs.size() do
15:    Iterator ← PolygonOne.find(temp)
16:    if Iterator then
17:      temp ← Iterator → second
18:      Contour.push_back(temp)
19:      PolygonOne.erase(Iterator           →
      first)
20:      Continue
21:    else
22:      Iterator           ←
        PolygonTwo.find(temp)
23:      temp ← Iterator → second
24:      Contour.push_back(temp)
25:      PolygonTwo.erase(Iterator           →
      first)
26:      end if
27:    end while
28:    Contours.push_back(Contour)
29:  end for
30: return Contours

```

4.2.3 Generation of the partitioned contours

After dividing the triangular meshes into different regions, we need to generate the outer contour of each partition and the

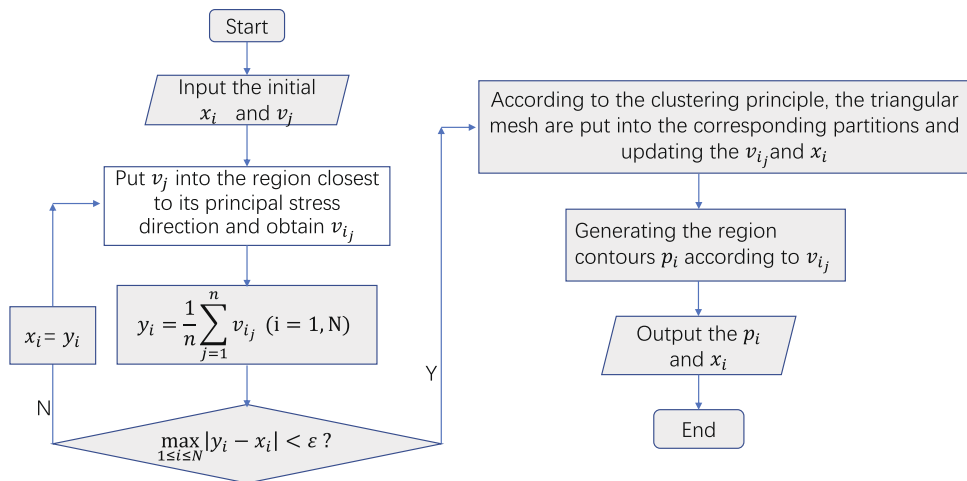
direction of the combined principal stress field of the partition for the generation of the filling path (Fig. 8). From the clustering method, it is clear that the line segments forming the outer contour of the partition must appear only once in the entire triangular meshes within the partition. If one line segment forms two triangles, then this line must not be the outer contour of the region. So you can determine whether this line forms the outer contour of the final partition by comparing the number of occurrences of the edges of triangular meshes in each partition. As shown in Fig. 9, these red line segments are shared by two adjacent triangles, so they should be removed from the set of line segments that make up the outer contour. As shown in the Algorithm 1, the input is a vector container that stores the triangulated meshes information. The output is also a vector container with the set of coordinates of points. Firstly, we adopt the function *ConvertTrianglesToSegs* to put each edge of the triangle into the set of line segments of the region and remove the duplicated line segments in each partition. The next step is to connect the line segments of each partition according to their adjacency. Two key-value data structures with opposite keys and values are generated for speeding up the searching process. Finally, the line segments can be joined into a complete outer contour by traversing the whole partition in the order of first and last.

4.3 Filling

After generating the outer contours of the partitions, we need to use a zigzag strategy to fill them according to the direction of the combined principal stress field of each partition, since the matrix expands from the nozzle to the two sides during the printing process. So the width of each side of the printing path is half of the nozzle diameter equal to D/2 (D is the nozzle diameter). So, to ensure the integrity of each zonal contour, we need to offset the outer contour inside each partition to avoid filling the outer boundary repeatedly.

Figure 10(a) shows the nozzle printing process, where the red line is the printing path and the white area is the printed area. Figure 10(b) shows the schematic diagram of the paralleled contour with offsets. The two dashed rectangles are the outer contour without offsetting and the rectangles in the blue region are the contour of the region after the offsetting. When the offset has been completed, the theoretical filling spacing between the outer contours of the region should be equal to the diameter of the nozzle. However, as verified by experimental printing, when the theoretical values are used for printing, large porosity appears at the intersection of the partition contours caused by the zigzag filling pattern. To eliminate this effect, our actual offsetting value should be less than D/2. This enhances the bonding of area boundaries during the printing process, allowing for tighter connections between areas. After the offset has been finished, we use the zigzag pattern to fill regions inside each partition according to its combined principal stress direction. Figure 11 shows the different filling

Fig. 7 Flow chart of region clustered



offsetting distances respectively. Figure 11(b) has been used for experiments to avoid poor filling quality.

5 Global path planning

Global path planning mainly uses inter-layer staggered filling to generate printing paths for processing transitional layers. It mainly includes three aspects, the generation of the printing path of transitional layers, compatibility between double layers, and connection from layer to layer.

5.1 Processing transitional layers filling

The processing transitional layer is mainly using a hybrid filling strategy with zigzag and contour-parallel filling patterns. First of all, to ensure the integrity of the entire filled area, it needs to print the outer boundary of the area using the contour-parallel methods. Then, it uses the outer contour after offsetting as the outer boundary of the partition. The main methods include the generation of offsetting paths, partitioning, and filling of regions.

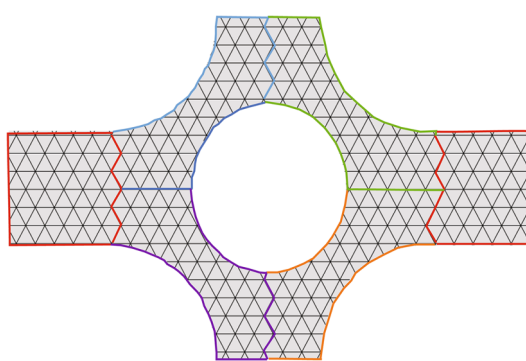


Fig. 8 Clustered contours

As shown in Fig. 12, the red line is the offsetting printing path, and the black line is the outer boundary of the inner filling. The offsetting distance of the red line segment is D (diameter of the nozzle), while the black offsetting distance is $3D/4$. This is because after the region splitting it is still necessary to offset $D/4$ inwards to ensure the tightness of the region connecting after the region splitting such as Fig. 11. The main method of filling the transitional layer is first to divide the area according to the direction of its minimum principal stress field. Then, it is to cluster these triangular meshes into a large region based on the process of Sect. 4.2 to generate filling paths with zigzag patterns. Figure 13 shows that (a) and (b) are the paths of filling regions with different distances of offsetting respectively. According to the experimental verification, the filling porosity due to the complex regional boundary contour can be reduced when using (b) filling methods. Due to the complex boundary morphology formed by the stress partitioning, the boundary filling does create instability when generating continuous zigzag filling paths, which may form large deposition spacing. To solve this issue, there are two options, one is to smooth the boundary. The other is to use inter-layer compensation to reduce the effect caused by uneven deposition spacing. In this paper, the second option is used by designing a double-layer collocation with adjacent layers of matrix material filling to compensate for the voids.

5.2 Compatibility between double layers

In this paper, the hybrid filling mode is used as a transitional layer to enhance the practical performance of the process. On the one hand, the hybrid filling mode can ensure the integrity of the outer contour boundary and increase the density of the filling, on the other hand, it can be perpendicular to the printing path of the reinforced layer, which can compensate for the porosity brought by the filling after partitioning, and also can further improve the bearing capacity through the mutual impregnation through the porosity.

Fig. 9 Schematic diagram of region merged

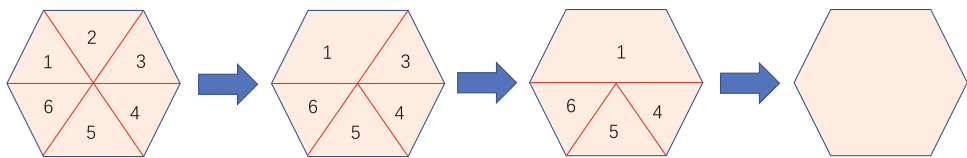


Fig. 10 Schematic diagram of nozzle printing. **a** Printing along the red line path. **b** Region offsetting

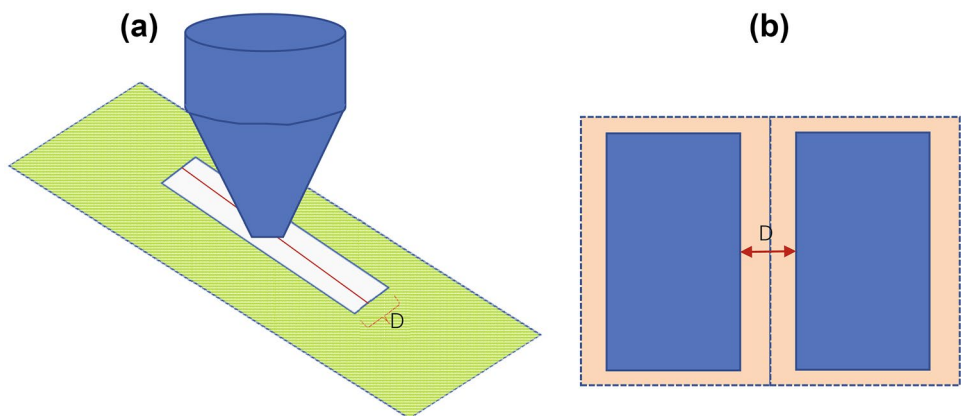


Fig. 11 Schematic diagram of offsetting. **a** Offset distance is equal to $D/2$. **b** Offset distance is equal to $D/4$. **c** Offset distance is equal to $D/6$. **d** Offset distance is equal to $D/8$

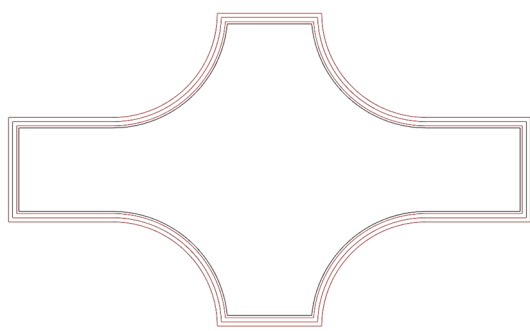
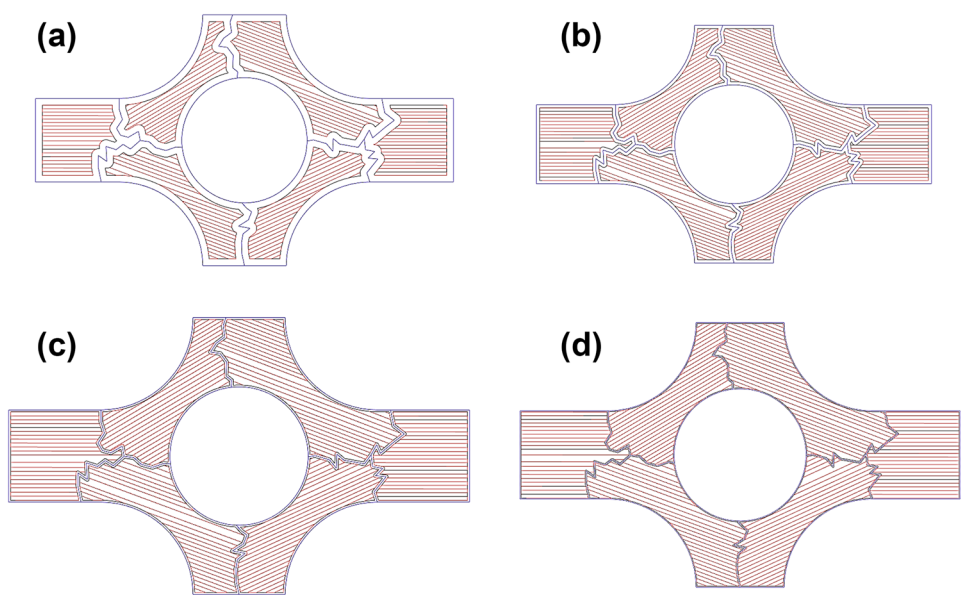


Fig. 12 Schematic diagram of contour offset

Transitional layers can also be filled with other filling strategies such as contour-parallel and Fermat's spiral curves. However, if using other filling modes, for one hand, it does not largely weaken the anisotropy of the FFF process due to the force field arrangement, and on the other hand, the strength may be further reduced due to the greater porosity. As shown in Fig. 14, Fig. 14(a) is filled with mixed vertical staggered filling, and Fig. 14(b) is filled with continuous Fermat's spiral curves. Since Fermat's spiral curve can not control its infill percentage, it is easy to cause a large porosity. Therefore, Fermat's spiral curves are generally not used as filling curves

Fig. 13 Schematic diagram of transition layer offset filling. **a** Offset distance is equal to $D/2$. **b** Offset distance is equal to $D/4$

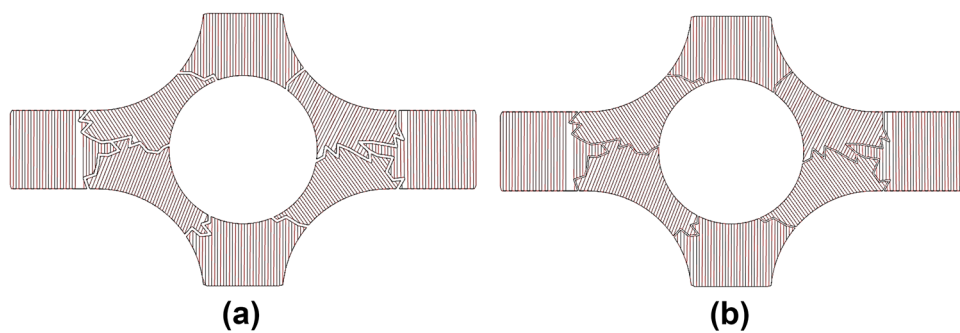
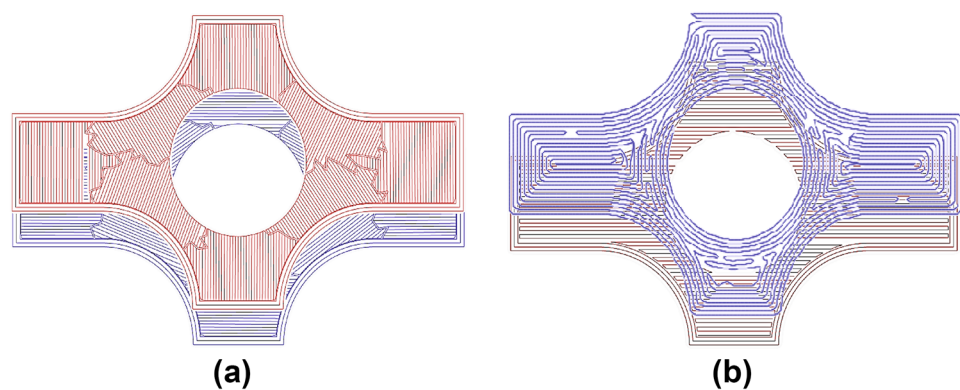


Fig. 14 Different transitional layer paths. **a** Transitional layer with vertical staggered filling. **b** Transitional layer with Fermat's spiral curve



for polymer printing. However, Fermat's spiral curve can be used as a transitional layer for global continuous filling printing for the continuous fiber-reinforced printing.

5.3 Inter-layer connection

Between the layers, we use the approximate nearest neighbor to find the two nearest points between the enhancement layer and the transitional layer as the starting and ending position of the inter-layer connection, which can effectively reduce the printing time and empty traveling distance. However, since each printed line segment initially consists of two endpoints

of the line segment, this is not favorable for finding the upper and lower adjacent points. So we interpolate the initial printing path equally so that the distribution of points on the line becomes dense. Figure 15(a) shows that the points A, B, C, and D on the blue line are the initial printing path points, and the points a, b, c, d, e, f, g, and h on the red line segment are the printing points after equivalent interpolation. The interpolated distance d is equal to $(l_{AB} + l_{BC} + l_{CD})/N$, where N is the total number of printing line segment. After equivalent interpolation of the path points, we can use the two points close to each other as the starting and ending points of the inter-layer connection according to the closest distance principle, thus forming

Fig. 15 Schematic diagram of inter-layer connections. **a** Interpolation for printing path. **b** IICP double-layer structure

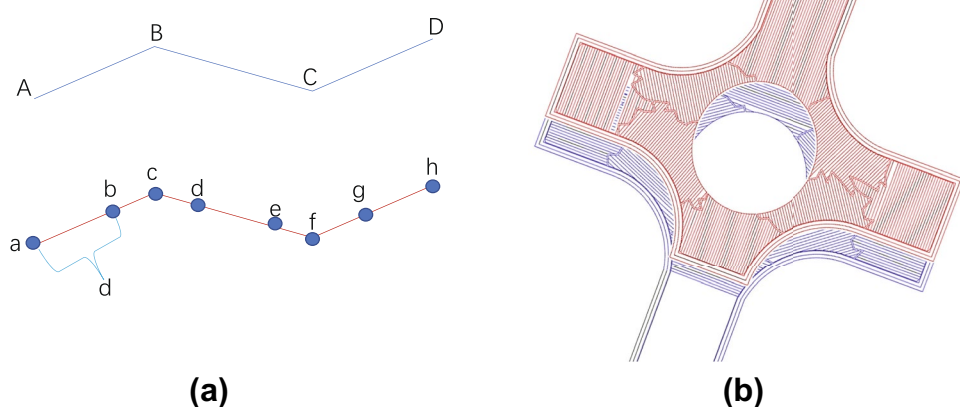
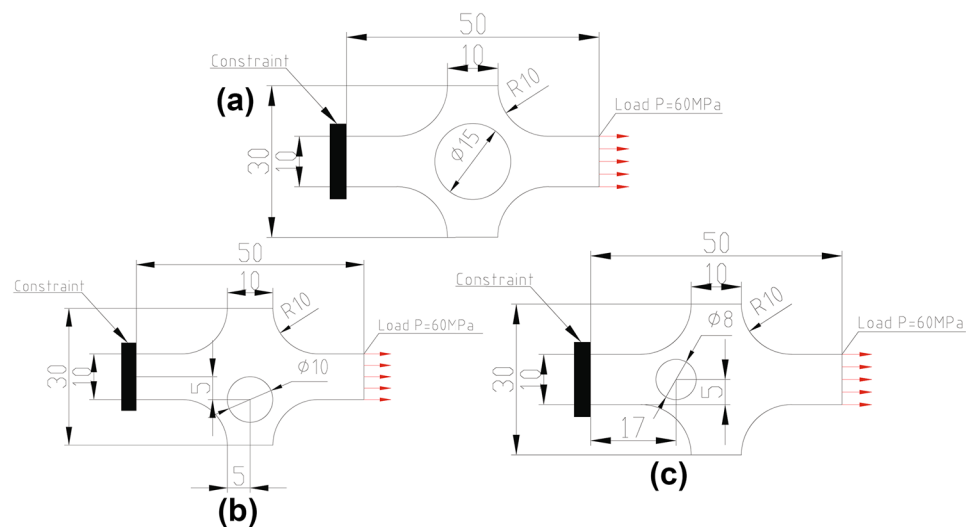


Fig. 16 Schematic diagram of three different model sizes and working conditions. **a** Model one. **b** Model two. **c** Model three



a double-layer connection between the enhancement layer and the processing transitional layer. As Fig. 15(b) shows, the entire three-dimensional space is filled by the double-layer continuous accumulation. This method is also suitable for continuous fibers as transitional layers to avoid repeated filling of fibers.

6 Experiment and discussion

The model dimensions and working conditions are shown in Fig. 16. The unit is millimeters and the thickness of the panel is 2 ml. Tetrahedral elements are used to divide the mesh, and their size is 0.5 mm. The loaded material is PLA

with the mechanical properties of density $\rho = 1.28 g/cm^3$, Young's modulus $E = 4000 MPa$, Poisson's ratio $\nu = 0.35$, and yield strength of 50 MPa. The side along the X-negative direction is a fixed constraint, and the side in the X-positive direction is loaded with a pressure of $P = 60 MPa$. Four different samples are used for the comparative tests for three different models as shown in Figs. 17, 18, and 19. The experiment was performed with a microcomputer-controlled material testing machine for the tensile test (2kN capacity, Shanghai songduan Manufacturing Co., Ltd). The loading speed is 5mm/min, and all results are the average of five sets of repeated tests.

Figure 20 shows printed and fractured samples of the three different models. The tensile testing results are shown

Fig. 17 IICP and three types of path filling forms for model one. **a** Filling paths used for Zigzag model with a filling angle of 0°. **b** Filling paths used for Zigzag model with a filling angle of 90°. **c** Filling paths used for Zigzag model staggered filling with 0 and 90°. **d** IICP

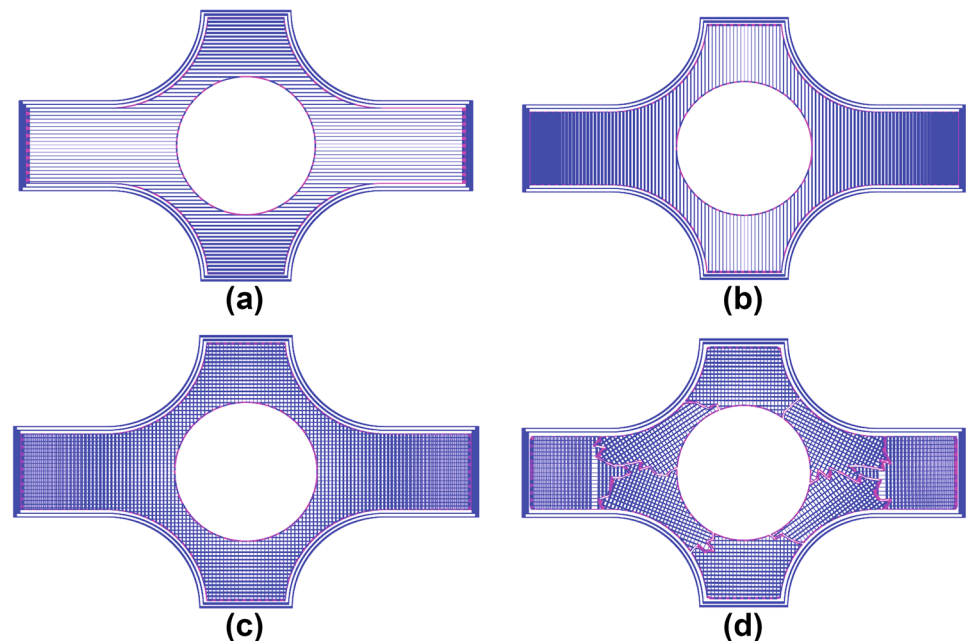
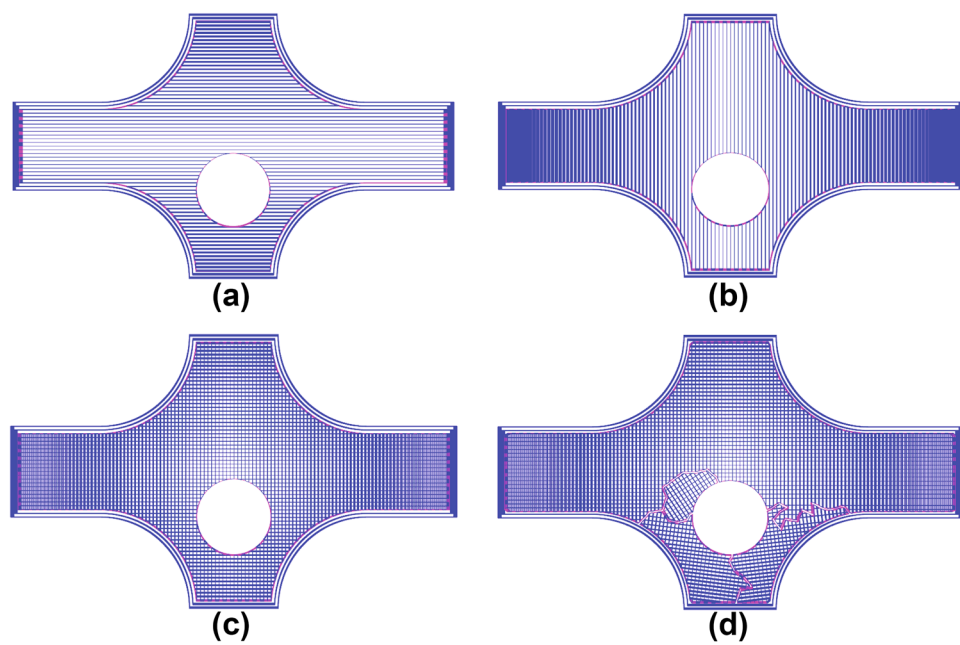


Fig. 18 IICP and three types of path filling forms for model two. **a** Filling paths used for Zigzag model with a filling angle of 0°. **b** Filling paths used for Zigzag model with a filling angle of 90°. **c** Filling paths used for Zigzag model staggered filling with 0 and 90°. **d** IICP



in Fig. 21, Tables 1, 2, and 3. The strength of the part printed by the IICP method is higher than the other filling methods. According to the location of the fracture in Fig. 20(b), (d), and (f), it can be seen that the part is most delicate near the hole, which is mainly due to the small cross-sectional area and weak load-bearing capacity here. But, we succeeded in separating these concentrated stresses and more fragile areas by using a filling along the principal stress direction of their areas employing the IICP method. In this way, the axial

direction of the filament printed in these areas along the load direction, in turn, makes the entire load capacity of the area stronger. In addition, continuous fiber-reinforced printing is also tested. The path is generated with the IICP method and printed on a common desktop FFF platform without fiber-cutting components. The printing result is shown in Fig. 22. The reinforcing material used in the experiment is continuous polyester fiber for sewing, and the matrix material is PLA.

Fig. 19 IICP and three types of path filling forms for model three. **a** Filling paths used for Zigzag model with a filling angle of 0°. **b** Filling paths used for Zigzag model with a filling angle of 90°. **c** Filling paths used for Zigzag model staggered filling with 0 and 90°. **d** IICP

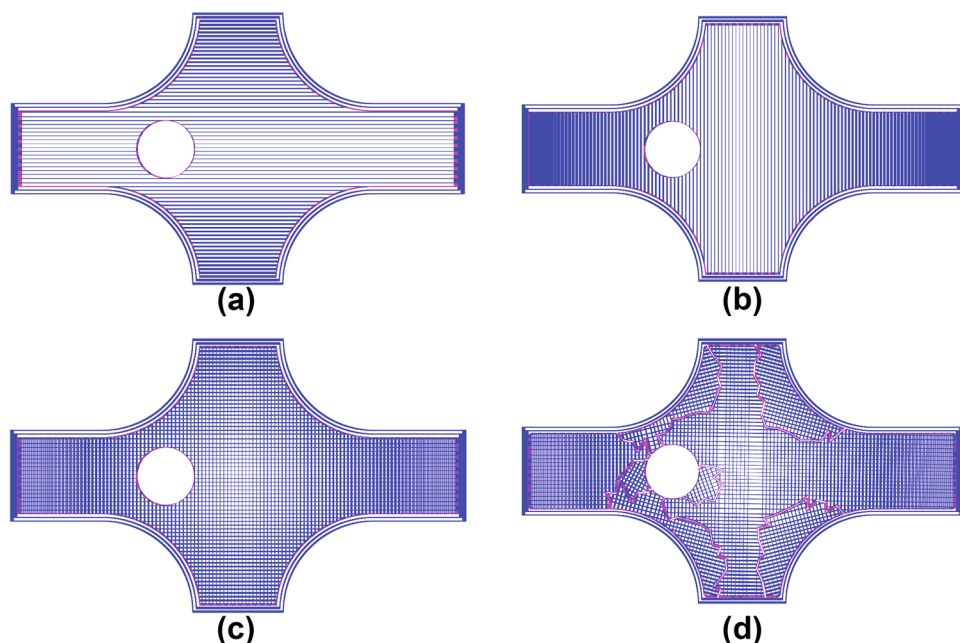


Fig. 20 Tensile test. **a** The samples printed according to the path generated in Fig. 17. **b** Fracturing model one after tensile test. **c** The samples printed according to the path generated in Fig. 18. **d** Fracturing model two after tensile test. **e** The samples printed according to the path generated in Fig. 19. **f** Fracturing model three after tensile test. **g** Tension machine

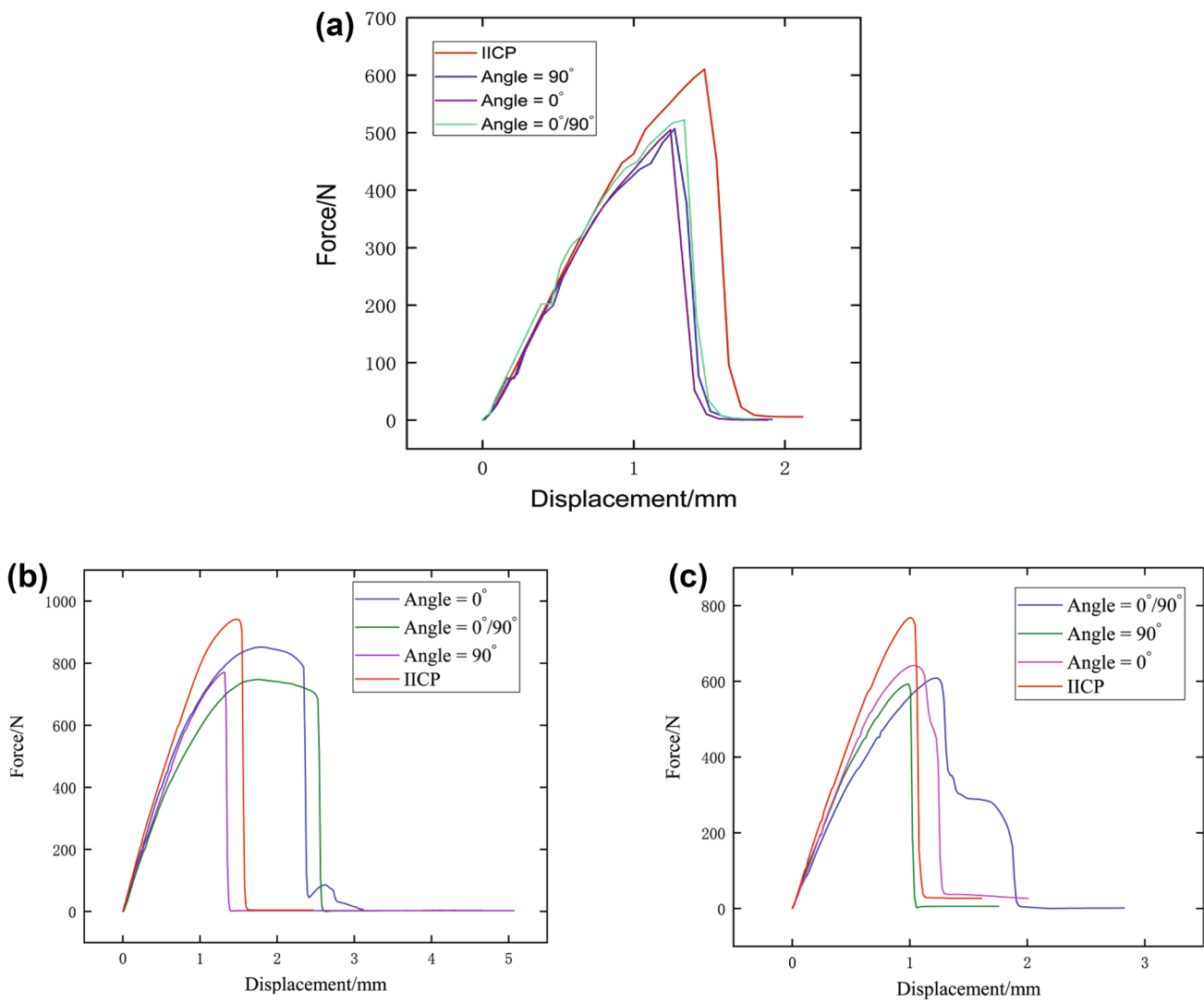
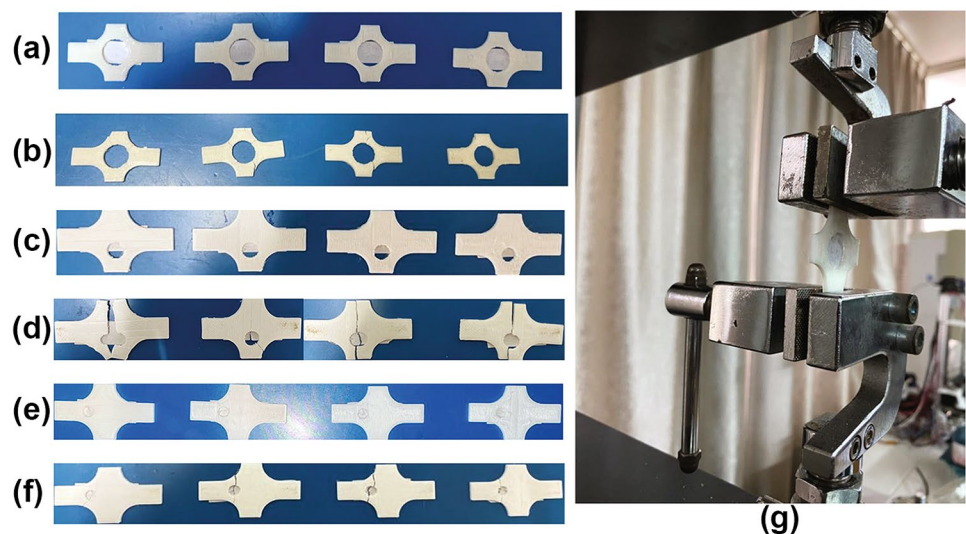


Fig. 21 Schematic diagram of tensile testing results. **a** Model one. **b** Model two. **c** Model three

Table 1 Features of model one fabricated by different tool-paths

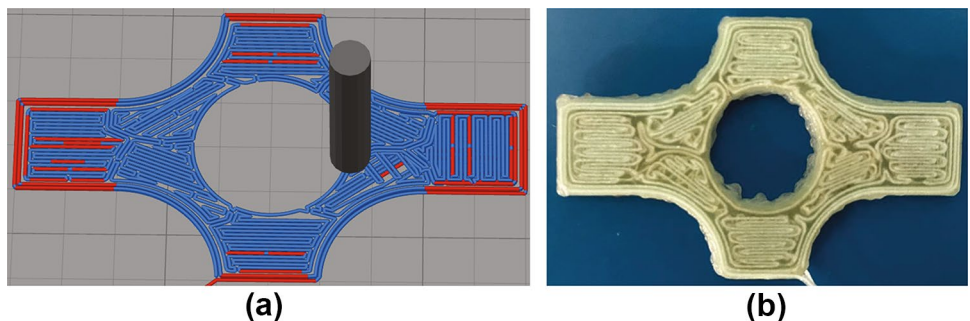
Physical quantities	Zigzag (0°)	Zigzag (90°)	Zigzag (0°/90°)	IICP
Ultimate force (N)	505.12	506.85	522.18	610.44 (+20.85%, +20.44%, +16.92%)
Measured mass (g)	1.8101	1.8469	1.8335	1.8440 (+1.87%, -0.16%, +0.57%)
Filament length (mm)	16,046.64	16,393.68	16,220.16	16,084.23 (+0.23%, -1.89%, -0.84%)

Table 2 Features of model two fabricated by different tool-paths

Physical quantities	Zigzag (0°)	Zigzag (90°)	Zigzag (0°/90°)	IICP
Ultimate force (N)	851.56	769.93	747.20	941.11 (+10.52%, +22.23%, 25.96%)
Measured mass (g)	1.8708	1.8904	1.8996	1.9252 (+2.91%, +1.84%, +1.35%)
Filament length (mm)	18,289.52	18,643.30	18,466.41	18,589.43 (+1.64%, -0.29%, +0.67%)

Table 3 Features of model three fabricated by different tool-paths

Physical quantities	Zigzag (0°)	Zigzag (90°)	Zigzag (0°/90°)	IICP
Ultimate force (N)	608.60	593.05	641.83	767.47 (+26.10%, +29.41%, +19.58%)
Measured mass (g)	1.9546	2.0415	1.9765	2.0136 (+3.0%, -0.14%, +1.88%)
Filament length (mm)	18,240.84	19,414.69	18,827.76	18,240.19 (+0.98%, -5.12%, -2.16%)

Fig. 22 Continuous fiber-reinforced printing. **a** IICP double-layer interleaved printing path. **b** IICP continuous fiber printed sample

7 Conclusion

This paper proposes an IICP planning method for the FFF process, which achieves targeted enhanced strength of printed parts through the printing path arrangement based on the partition of the direction of the principal stress field. It enhances the practical performance of the FFF process by reducing its anisotropy through vertically staggered filling between layers. Compared to traditional filling methods such as the zigzag filling strategy, the strength of the printed part is increased by 10 to 30%. The IICP method has the following advantages.

- Based on the stress field partitioning printing method, it can effectively perform enhancement in different regions. Compared with existing planning methods,

partition fitting enhancement can increase the stability of path planning.

- The design of the double-layer structure increases the inter-layer connection performance and compensates for the porosity generated by the uneven deposition spacing.
- The continuous path planning can be further adapted to continuous fiber-reinforced printing to utilize the mechanical properties of high-performance fibers.

Since all the methods used in this paper are generalized, such as finite element analysis and zigzag filling strategy, this makes the IICP method in this paper not only applicable to the analysis under arbitrary working conditions, but can also be integrated into general CAE analysis software.

In IICP, sliced layers are divided into different stress regions to achieve mechanically enhanced printing paths,

so the boundaries of the partitions will have significant cracks, which will affect the filling quality and density. In addition, the IICP method generates the printing paths based on the stress field in specific working conditions, thus limiting the application of the IICP method for printed parts. These issues still need further optimization and improvement. If the continuous fiber-reinforced printing path is required, the transitional layer can be filled not only with a continuous zigzag curve but also with a Fermat's spiral curve, or even with a mixture of continuous zigzag and Fermat's spiral curves. Therefore, the IICP planning method proposed in this paper is not only easy to apply in existing polymer printing processes but also can be extended to apply to continuous fiber-reinforced manufacturing.

Author Contributions Yuan Yao presented the basic framework and key concepts of the article and made the first version manuscript of this paper. Hang Zhang designed the algorithms, experiments, and the drafted article. Yingxin Ma implemented part of the article's algorithm. Maximilian Lackner and Yunliang Jiang made the critical revision of the paper.

Funding This work is partially supported by the Nano-Science and Technology Research Center at Shanghai University and the Austrian Research Promotion Agency (the Natural 3D project 860384 grant).

Availability of data and material Not applicable.

Code availability The C++ implementation of Algorithm 1 and the source code of the entire process have been opened on Github and can be accessed through [github](#).

Declarations

Ethics approval and consent to participate Not applicable.

Consent for publication Not applicable.

Conflict of interest The authors declare no competing interests.

References

- Pan W, Wang S, Zhang X, Lu WF, Wang Y, Jiang H (2022) A kinematics-aware decomposition approach for complex CAD parts in additive manufacturing. *Addit Manuf* 50:102493
- Bhushan B, Caspers M (2017) An overview of additive manufacturing (3D printing) for microfabrication. *Microsyst Technol* 23(4):1117–1124
- Praveena BA, Lokesh N, Abdulrajak B, Santhosh N, Praveena BL, Vignesh R (2021) A comprehensive review of emerging additive manufacturing (3D printing technology): methods, materials, applications, challenges, trends and future potential. *Materials Today: Proceedings*
- Kareem FA, Michael PA (2022) An investigation on applications of additive manufacturing of electrical machines. *Materials Today: Proceedings*
- Vishwas M, Basavaraj CK (2017) Studies on optimizing process parameters of fused deposition modelling technology for ABS. *Materials Today: Proceedings* 4(10):10994–11003
- Cano-Vicent A, Tambuwala MM, Hassan SS, Barh D, Aljabali AAA, Birkett M, Arjunan A, Serrano-Aroca Á (2021) Fused deposition modelling: current status, methodology, applications and future prospects. *Addit Manuf* 47:102378
- Agarwal KM, Shubham P, Bhatia D, Sharma P, Vaid H, Vajpeyi R (2022) Analyzing the impact of print parameters on dimensional variation of ABS specimens printed using fused deposition modeling (FDM). *Sensors International* 3:100149
- Parulski C, Jennotte O, Lechanteur A, Evrard B (2021) Challenges of fused deposition modeling 3D printing in pharmaceutical applications: where are we now? *Adv Drug Deliv Rev* 175:113810
- Ćwikla G, Grabowik C, Kalinowski K, Paprocka I, Ociepka P (2017) The influence of printing parameters on selected mechanical properties of FDM/FFF 3d-printed parts. In: IOP Conference Series: Materials Science and Engineering, vol 227. IOP Publishing, p 012033
- Vishwas M, Basavaraj CK (2017) Studies on optimizing process parameters of fused deposition modelling technology for ABS. *Materials Today: Proceedings* 4(10):10994–11003. Advanced Materials, Manufacturing, Management and Thermal Science (AMMMT 2016) September 23–24, 2016
- Galetto M, Verna E, Genta G (2021) Effect of process parameters on parts quality and process efficiency of fused deposition modeling. *Comput Ind Eng* 156:107238
- Tian X, Liu T, Yang C, Wang Q, Li D (2016) Interface and performance of 3D printed continuous carbon fiber reinforced PLA composites. *Compos Part A: Appl Sci Manufac* 88:198–205
- Fischer D, Eßbach C, Schönher R, Dietrich D, Nickel D (2022) Improving inner structure and properties of additive manufactured amorphous plastic parts: the effects of extrusion nozzle diameter and layer height. *Addit Manuf* 51:102596
- Zhang J, Wang XZ, Yu WW, Deng YH (2017) Numerical investigation of the influence of process conditions on the temperature variation in fused deposition modeling. *Mater Des* 130:59–68
- Ansari AA, Kamil M (2021) Effect of print speed and extrusion temperature on properties of 3D printed PLA using fused deposition modeling process. *Materials Today: Proceedings* 45:5462–5468. Second International Conference on Aspects of Materials Science and Engineering (ICAMSE 2021)
- Go J, Hart AJ (2017) Fast desktop-scale extrusion additive manufacturing. *Addit Manuf* 18:276–284
- Dai S, Deng ZC, Yu YJ, Zhang K, Wang SH, Ye J (2020) Orthotropic elastic behaviors and yield strength of fused deposition modeling materials: theory and experiments. *Polym Test* 87:106520
- Ding D, Pan ZS, Cuiuri D, Li H (2014) A tool-path generation strategy for wire and arc additive manufacturing. *Int J Adv Manuf Technol* 73(1–4):173–183
- Ren F, Sun Y, Guo D (2009) Combined reparameterization-based spiral toolpath generation for five-axis sculptured surface machining. *Int J Adv Manuf Technol* 40(7–8):760–768
- Shaikh S, Kumar N, Jain PK, Tandon P (2016) Hilbert curve based toolpath for FDM process. In: CAD/CAM, Robotics and Factories of the Future. Springer, pp 751–759
- Jin GQ, Li WD, Gao L (2013) An adaptive process planning approach of rapid prototyping and manufacturing. *Robot Comput Integr Manuf* 29(1):23–38
- Lin S, Xia L, Ma G, Zhou S, Xie YM (2019) A maze-like path generation scheme for fused deposition modeling. *Int J Adv Manuf Technol* 104(1):1509–1519
- Lin Z, Jianzhong Fu, He Y, Gan W (2013) A robust 2D point-sequence curve offset algorithm with multiple islands for contour-parallel tool path. *Comput Aided Des* 45(3):657–670

24. Zhao H, Chen B, Gu F, Huang QX, Garcia J, Yong C, Tu C, Benes B, Hao Z, Cohen-Or D (2016) Connected Fermat spirals for layered fabrication. *ACM Trans Graph* 35(4):1–10
25. Koch C, Van Hulle L, Rudolph N (2017) Investigation of mechanical anisotropy of the fused filament fabrication process via customized tool path generation. *Addit Manuf* 16:138–145
26. Bendsoe MP, Sigmund O (2003) Topology optimization: theory, methods, and applications. Springer Science & Business Media
27. Papapetrou VS, Patel C, Tamjani AY (2020) Stiffness-based optimization framework for the topology and fiber paths of continuous fiber composites. *Compos Part B Eng* 183:107681
28. Tam K-MM, Mueller CT (2017) Additive manufacturing along principal stress lines. *3D Printing and Additive Manufacturing* 4(2):63–81
29. Kubalak JR, Wicks AL, Williams CB (2019) Deposition path planning for material extrusion using specified orientation fields. *Procedia Manufacturing* 34:754–763. 47th SME North American Manufacturing Research Conference, NAMRC 47. Pennsylvania, USA
30. Sales E, Kwok T-Ho, Chen Y (2021) Function-aware slicing using principal stress line for toolpath planning in additive manufacturing. *J Manuf Process* 64:1420–1433
31. Li Y, Ke Xu, Liu Xu, Yang M, Gao J, Maropoulos P (2021) Stress-oriented 3D printing path optimization based on image processing algorithms for reinforced load-bearing parts. *CIRP Ann* 70(1):195–198
32. Jin Y, He Y, Guoqiang Fu, Zhang A, Jianke Du (2017) A non-retraction path planning approach for extrusion-based additive manufacturing. *Robot Comput Integr Manuf* 48:132–144
33. Ahn S-H, Montero M, Odell D, Roundy S, Wright PK (2002) Anisotropic material properties of fused deposition modeling ABS. *Rapid Prototyp J*
34. McLouth TD, Severino JV, Adams PM, Patel DN, Zaldivar RJ (2017) The impact of print orientation and raster pattern on fracture toughness in additively manufactured ABS. *Addit Manuf* 18:103–109
35. Fang G, Zhang T, Zhong S, Chen X, Zhong Z, Wang CCL (2020) Reinforced FDM: multi-axis filament alignment with controlled anisotropic strength. *ACM Transactions on Graphics (TOG)* 39(6):1–15
36. Minetto R, Volpatto N, Stolfi J, Gregori RMMH, da Silva MVG (2017) An optimal algorithm for 3D triangle mesh slicing. *Comput Aided Des* 92:1–10

Publisher's Note Springer Nature remains neutral with regard to jurisdictional claims in published maps and institutional affiliations.

Springer Nature or its licensor holds exclusive rights to this article under a publishing agreement with the author(s) or other rightsholder(s); author self-archiving of the accepted manuscript version of this article is solely governed by the terms of such publishing agreement and applicable law.